


# CFD analysis and optimization of axial flow fans

Renhui Liu<sup>1</sup>, Shubo Xu<sup>1,\*</sup> , Kangwei Sun<sup>1</sup>, Xiaoyu Ju<sup>1</sup>, Weihai Zhang<sup>2</sup>, Wenming Wang<sup>3</sup>, Xiquan Ma<sup>1</sup>, Yuefei Pan<sup>1</sup>, Jianing Li<sup>1</sup>, and Guocheng Ren<sup>1</sup>

<sup>1</sup> Shandong Jianzhu University, School of Materials Science and Engineering, Jinan 250101, China

<sup>2</sup> Weifang Fuyuan Supercharger Co., LTD, Weifang, 261206, Shandong, China

<sup>3</sup> Shandong Wenling precision forging Technology Co., LTD, Jinan, 271100, Shandong, China

Received: 19 January 2024 / Accepted: 4 April 2024

**Abstract.** The axial fan plays a vital role in the safe production of the mine, and in this paper, a mine axial flow ventilator is designed through numerical simulation to meet the demand of air exchange inside and outside of the mine, so as to maintain the oxygen supply of the mine and discharge the harmful gases. Finite element analysis of four structural factors of axial fan blade installation angle, number of blades, deflector plate, rotational speed, drawing fan wind pressure and rotational speed cloud diagram, calculation of axial power, by analyzing the distribution of the cloud diagram to design the shape of the fan blade, and derive the change rule of the wind pressure when changing the structure of the fan. By using gradient descent method to control the percentage of imported mass flow rate, the P-Q performance curve of the fan is obtained, which optimizes its aerodynamic performance, improves efficiency, and extends its service life.

**Keywords:** Axial fan / finite element analysis / structural optimization / performance curves / aerodynamic performance

## 1 Introduction

In the fluid simulation of axial fans, the CFD (Computational Fluid Dynamics) method is usually used to numerically simulate the fluid inside the fan [1]. CFD simulation of axial fans can be used to obtain the aerodynamic performance data of the fan, such as air volume, pressure, efficiency, etc., so that the fan design can be evaluated and optimized [2]. In the CFD simulation of an axial fan, the factors to be considered include the shape, angle [3], and materials [4] of the fan blades, as well as the parameters such as the fan's speed, flow rate, and pressure [5]. It is also necessary to consider the characteristics of the fluid medium, such as density, viscosity, and thermal conductivity [6,7]. In this paper, the aerodynamic performance of axial fan will be studied with axial fan blade mounting angle, number of blades, deflector, and fan speed as variables, and the optimal structure will be sought by changing the above parameters in order to achieve the optimal aerodynamic performance within a limited range, which will provide a theoretical basis for the subsequent research.

China is rich in mineral resources due to its favorable geographical location [8]. One of the problems involved in the mining of mineral resources is safety, and good

ventilation of the mine can effectively reduce the occurrence of safety accidents [9]. The axial fan shown in Figure 1 is currently the main tool for ventilation in small and medium sized mines. In order to meet the requirements for use and to develop new products, scientists in various fields have carried out a lot of research and obtained the corresponding results. Yang et al. [10] used Finite Volume Analysis software to analyze the tunnel axial fan and obtained the relationship between the total pressure and efficiency of the fan under different blade installation angles and different flow conditions. By analyzing the above data, the optimal working area of the turbine was determined to provide guidance to the researchers. In addition, some researchers have carried out CFD simulation studies on axial fans and proposed a new design using different number of blades, and the numerical results show that this design has better performance [11]. On fan guide vanes, Wang et al. [12] conducted numerical simulations and experimental validation studies for axial fans with relatively small hubs. The circular rear guide vanes were found to improve the aerodynamic performance of the fan, and the original blades with aerodynamically shaped blade sections represent the performance of the fan blades. Liu Yang [13] and others designed the mounting angle of the guide vane on the casing, performed the N-S equation combined with turbulence modeling, and concluded that the angle of 60° is the best inlet guide vane. After installing

\* e-mail: [xsb@sdjzu.edu.cn](mailto:xsb@sdjzu.edu.cn)

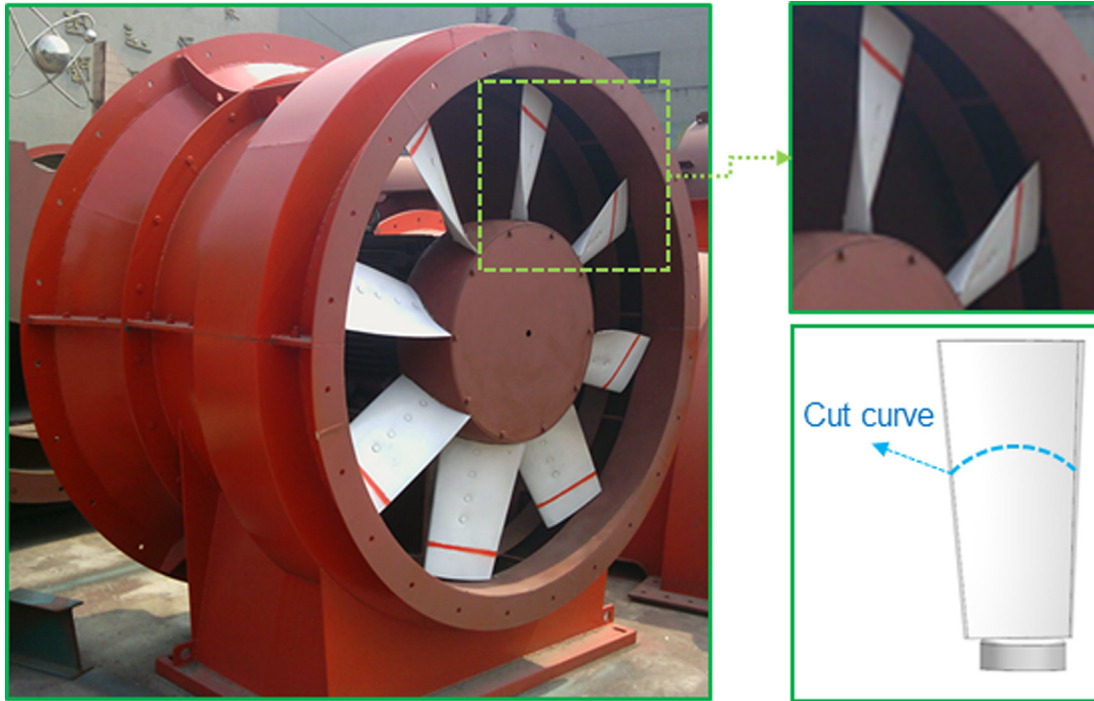


**Fig. 1.** Mining axial fan.

this guide vane, the static characteristics of the axial fan were significantly improved. Munisamy et al. [14] used the commercial software ANSYS FLUENT to analyze the good results brought about by the use of stator blades with the same profile as the rotor blades as an outlet guide vane in the opposite direction before encountering the rotational effects and velocity vector deflections induced by the rotor blades in a medium sized axial fan with different pitch blades. Wu et al. [15] used an axial fan as a research object, and through numerical simulation of three different airfoil types (straight, C-type, and forward-swept blades), they obtained the results that under the same operating conditions, the forward-swept fan has the highest total pressure efficiency, the C-type blade has a slightly lower efficiency, and the straight blade has the lowest efficiency. And the airfoil shape of the blades was optimized by orthogonal optimization method. Liu and others [16] used to set the flow resistance in the downstream region of the computational domain to reduce the deviation between the simulation and experimental results, and then investigated the effect of blade angle of attack on the performance of axial fan, they found that the blade flow pattern is extremely sensitive to the change of blade angle of attack, and the change of the blade angle of attack will lead to a large change of the performance of the fan in different states, especially in the tip region, lateral flow will appear or even backflow. Yu et al. [17] achieved the optimum aerodynamic performance of the fan by adjusting the angle of the blades at rest and matching the fan speed at the same time. During the design process, various techniques were applied and the stiffness problem of the hub due to the weight of the blades, torque, etc. was solved. The design of this design of the dynamic blade adjustable axial fan can be operated stably for a long period of time. Diao Lei et al. [18]

investigated the internal flow characteristics of the flow field by exploring three different models and experimentally verifying the model while adopting the method of tip splitting. They found that the three different models showed gas leakage and pressure loss in different regions, but the model characters had corresponding advantages, and they also investigated the effect of noise to obtain the relevant laws. After the study of the structure, Podgaietsky Gabriel and others [19] created a new method of mapping the efficiency of axial fans, they pointed out that, through the method of blade elements, and the finite elementization of the blades for the study, through the study of the efficiency of the electric motor and the blades to get the source of the irreversible losses and the reasons for the uneven distribution of the flow rate, and then through the change of the fan parameters to optimize the design to get a high-efficiency fan. Parameters of the fan and then optimize the design to obtain a high-efficiency fan. Salcedo et al. [20] investigated a wireless remote controlled axial fan with the remote control part at the blade pitch as well as at the air outlet, they characterized two sizes of air outlets as well as three sizes of blade-to-blade pitch and concluded that the airflow is relatively small at small outlet sizes while the opposite is true for hitting outlets, and that the larger the model with the larger blade pitch, the higher the exit velocity. Pogorelov Alexej et al. [21] by performing a large eddy simulation of the flow field of a 5-bladed axial fan and solving for individual blades using new periodic boundaries, obtained that the internal flow field of the fan changes and a complete turbulence inversion occurs when the blade gap is reduced, in addition to reducing the magnitude of the vortex drift at the end gap when the top of the blades gap is reduced, in addition to this they also did an analysis of the acoustic field. Ye Xuemin et al. [22] by changing the shape

**Table 1.** Mining axial fan parameters.

Parameter names	Parameter
Fan size(mm)	1320
Mounting angle (°)	0/5/15/20/25
Blade curvature (°)	5.3
Wheel ratio (*)	0.42
Blade number	8/9/10
Spoiler	Ahead/offside/ahead and back

of the blade tip structure and using Fluent to analyze the Finite Volume Simulation of different structures, they found that the total pressure and axial power of the turbine assembled with grooved blade tips are smaller than the original turbine, while the leakage of the internal flow is significantly reduced due to the blade's perturbation to the internal flow field. The efficiency of the blade is improved by 1.07% year-on-year, which effectively improves the performance of the turbine. Moghadam Seyed Mohsen Alavi et al. [23] performed large vortex simulations for six configurations of three blade top clearances to analyze the effect of three factors on the flow field inside the fan in terms of mean transient flow field. It was found that the angle between the blade chord and the tip leakage vortex decreases as the blade top clearance increases. The results show that the axial velocity maximum and turbulent kinetic energy as well as its relative reduction with losses when the size of the blade top clearance decreases under the set operating conditions. Li-Min et al. [24] showed that due to the unstable working condition of mining axial fans under low flow velocity conditions, the safety and reliability of the fans during operation were greatly reduced. Therefore, they investigated and solved the above problem through simulation studies combined with visualization techniques, and in order to improve the quality of the internal flow at low flow velocities, they designed a blade separator and an internal flow separator. It is found that the above design effectively improves the internal flow field condition of the low-speed axial fan and enhances its aerodynamic performance. In addition, there is no lack of more excellent scholars at home and abroad to provide more excellent results [25–30], which will not be listed in this paper, and the research results mentioned in this paper are not systematic enough although they are already relatively mature, so this study will further investigate the structural optimization of wind turbines.

## 2 Finite volume model

### 2.1 Geometric model

The focus of this study is to investigate the effect of structural parameter variations on the aerodynamic performance of mining axial fans. Three groups of research variables, namely, blade mounting angle, number of blades, and deflector, were set up for the study, while the same hub diameter was set up for each group to ensure the uniformity of the variables. The parameters are shown in Table 1.

The blade is made of ZL104 aluminum alloy melt die casting, with a height of 420 mm. The material used for the hub is cast iron, the hub wall thickness is 10 mm, due to the poor casting process caused by the uneven surface morphology of the blade is not counted in the calculation results. In Figure 2, (a) is a die cast aluminum alloy blade, and a small amount of burrs and burrs can be seen at the edge of the blade. (b) For the 3D model of the blade, the commercial 3D modeling software NX12.0 was used for design, which removed the above-mentioned adverse factors of the die cast blade to improve the quality of the grid, thereby improving the accuracy and efficiency of the calculation.

### 2.2 Mathematical modeling

In this study, the three-dimensional N-S equations are computed in the incompressible fluid domain, and the turbulence model is chosen to be k- $\epsilon$ , with the rotating wall reinforced by an augmented wall function. The inlet of the fluid domain is set as mass-flow inlet, the outlet is set as pressure outlet, and the fan is set to rotate around the Z-axis in the negative direction in the standard coordinate system (Frame motion). At the same time the wall is selected as a rotating wall, the Enhanced Wall Function is checked, and the direction is the same as the direction of rotation of the fan. The numerical simulation method is SIMPLEC and the N-S equations are solved using the second order windward format.

### 2.3 Optimize workflow

The research methodology used in this study is carried out on a case-by-case basis, where a good three-dimensional model is constructed first, and then the fluid domain is constructed, the mathematical model is based on the function of the software, and the corresponding results are obtained through Finite volume analysis of various structural models, and the optimized structure is optimized through the comparison of the data to obtain the optimal wind turbine model, which is used in the production and life. Figure 3 shows the optimization workflow used in this study.

### 2.4 Computational model

Fluid domains are created by simplifying the model in SpaceClaim, mainly including inlet, rotation and outlet domains. According to the fan P-Q curve simulation approach, the diameter of the inlet domain and outlet domain is 2 times of the rotating domain, and the length is 5 and 10 times of the diameter of the rotating domain, respectively. For the rotating domain of the fan, the Boolean subtraction operation in SpaceClaim will subtract the entity of the fan to leave the rotating domain, and the interiors are used to connect the rotating domain and the inlet/outlet basins, to ensure that the air is not leaked during the simulation. The rotational domain and the inlet and outlet basins are connected using interior to ensure

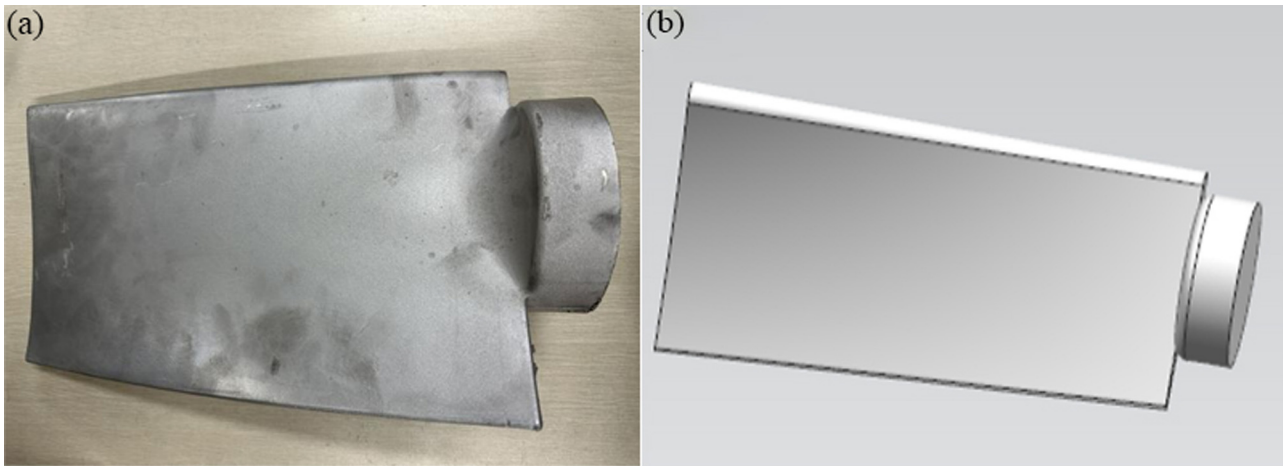


Fig. 2. Solid blade (a) and blade 3D modeling (b).

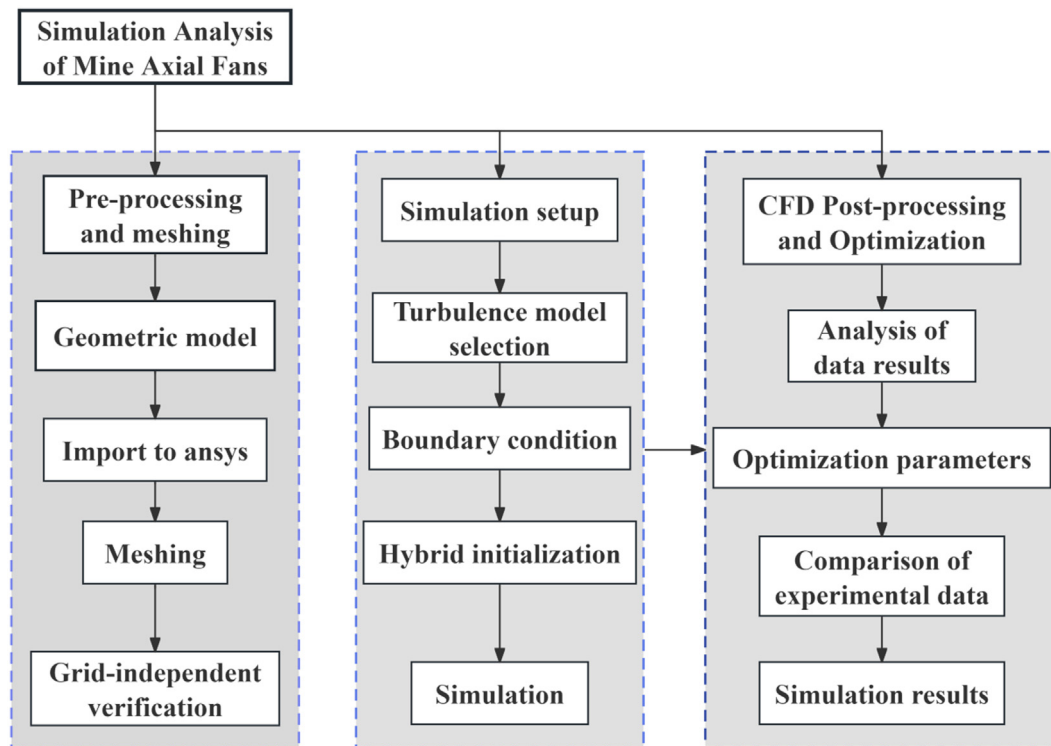


Fig. 3. Optimize workflow.

that air does not leak during the simulation. The relative error between the simulated and experimental results of this modeling method is small.

## 2.5 Mesh division

Grid in the fluid calculation is a crucial step, the grid is good or bad to determine the accuracy and speed of the calculation, due to the presence of axial fan blade and hub complex three-dimensional structure, in the division in order to ensure the quality of the grid of these areas using unstructured grid, the rest of the part of the structured mesh, such as inlet computational domain extension

domain and outlet computational domain extension domain. In addition, unstructured meshing is also required at the computational domain junction, while a reasonable boundary layer is set at the junction. In this study, the computational grid of axial flow fans was automatically divided using the grid division module ICEM in Fluent. The grid size is verified through grid independence, and the final grid size for the inlet and outlet domains is determined to be 50 mm. The remaining grids are set to the global grid size, and the size is automatically controlled by the software. In order to further improve the accuracy of the calculation, the rotating domain of the fan is encrypted, the grid size is set to 10 mm, and the mesh size at the blade



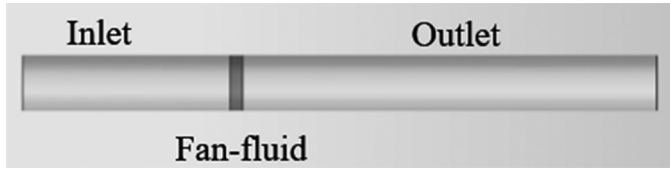


Fig. 4. Axial fan calculation domain.

and chamfer is 5 mm. Through the above grid partitioning process, an excellent computational grid can be obtained, and the local grid cross-section (the local positions of the inlet and outlet domains, as well as the rotation domain in Fig. 4) is shown in Figure 5.

## 2.6 Grid-independent verification

Since the paper involves the variation of grid sizes, in order to improve the efficiency of the calculation, the grid generation is performed for different grid sizes respectively, and three results are obtained, which are 5,690,000 for the number of Grid 1, 7,200,000 for the number of Grid 2, and 10,560,000 for the number of Grid 3. For 2000 iterations of calculation for the three grid sizes, the computation time of Grid 1 is 10 h, the computation time of Grid 2 is 9.3 h, and the Grid 3 The computation time is 15 h for Grid 1, 9.3 h for Grid 2, and 15 h for Grid 3. The relative error of the three results is 0.5%. Therefore, in a comprehensive view, choosing Grid 2 gives fast calculation results with high accuracy.

## 3 Calculation settings and boundary conditions

The axial fan in this study works in a humid underground environment and requires a large air volume as well as air pressure. According to the usage scenario, use the mass flow inlet, pressure outlet boundary conditions, consider the compressibility of air, select Reference Frame, set the rotation axis as Z-axis, the direction as  $-1$ , change the unit of rotational speed to rpm, and set the fluid medium as air, the density as  $1.225 \text{ kg/m}^3$ , and the viscosity as  $1.7894 \times 10^{-5} \text{ kg/(m*s)}$ . The fluid simulation process of rotating machinery involves two main regions, namely the rotating domain (impeller) and the fluid domain (inlet and outlet extension domain). The impeller rotates around the main axis and is coupled using a multiple reference system (MRF), which defines the center of rotation of the impeller as  $(0, 0, 0)$ . For the simulation, the rotational speed is set to 1450 rpm, Rotational is checked, the wall is set as a sliding wall, the rotational speed is set to 0 rpm, and the direction of rotation is the Z-axis, and the direction is kept the same as the direction of rotation of the wheel hub, which is  $-1$ . The remaining surfaces are all fixed wall surfaces.

To solve the calculation, the solution function is set to SIMPLEC. Firstly, the first order windward format is used to solve the problem, and when the convergence curve is observed to converge (The standard for calculating curve convergence in this study is that the curve exhibits the

same trend of change within 10 iteration cycles. As shown in Fig. 6), the calculation is stopped and the second order windward format is used to discretize the basic system of equations, and the maximum flow rate of the wind turbine is determined after the initial calculation, which is used as the initial value of the calculation. This study used the percentage subtraction method for the initial maximum flow rate, reducing the inlet flow rate by 10% each time. By controlling the inlet mass flow rate, the relationship between outlet flow rate, outlet pressure, and outlet velocity was obtained at different inlet flow rates. When conducting finite volume simulation calculations, various parameters including the number of blades, front and rear guide vanes, etc. will be most variable related to the results of the above simulation. The total number of iterations for simulation calculation is 2000, with a step size of 0.1. The number of iterations set in the Fluent settings panel is 200. Algebraic equation iterations were calculated in a Subrelaxation Manner, and the convergence accuracy was set to  $10^{-3}$  for the residual curve. At the same time, in order to observe the internal state of the axial flow fan more intuitively during simulation calculation, an observation surface is set in the  $x y$  plane, and three characteristics of pressure, velocity, and velocity vector are assigned to the observation surface. In addition, the axial flow fan as a whole is considered as a research object, and pressure characteristics are assigned to its surface, which will be recorded in the simulation calculation results.

## 4 System of turbulence equations

### 4.1 Law of Conservation of Mass

In the right-angle coordinate system, the continuity equation of fluid motion can be obtained, and its differential form is shown in (1):

$$\frac{\partial \rho}{\partial t} + \frac{\partial(\rho u)}{\partial x} + \frac{\partial(\rho v)}{\partial y} + \frac{\partial(\rho w)}{\partial z} = 0. \quad (1)$$

Equation (1) is given by the dispersion formula:

$$\text{div}(\rho V) = \frac{\partial(\rho u)}{\partial x} + \frac{\partial(\rho v)}{\partial y} + \frac{\partial(\rho w)}{\partial z}. \quad (2)$$

Equation (2) can also be simplified as:

$$\frac{\partial \rho}{\partial t} + \text{div}(\rho V) = 0. \quad (3)$$

Equation (3) is a constant when the fluid is incompressible, so equation (1) can be expressed as equation (4):

$$\frac{\partial(\rho u)}{\partial x} + \frac{\partial(\rho v)}{\partial y} + \frac{\partial(\rho w)}{\partial z} = 0. \quad (4)$$

In equation (4).  $\rho$ —representative density;  $t$ —representative time;  $V$ —Represents the velocity vector, and can be expressed as  $V = ui + vj + wku$ ,  $v$ ,  $w$  are the velocity components of the velocity in the  $X, Y, Z$  axes

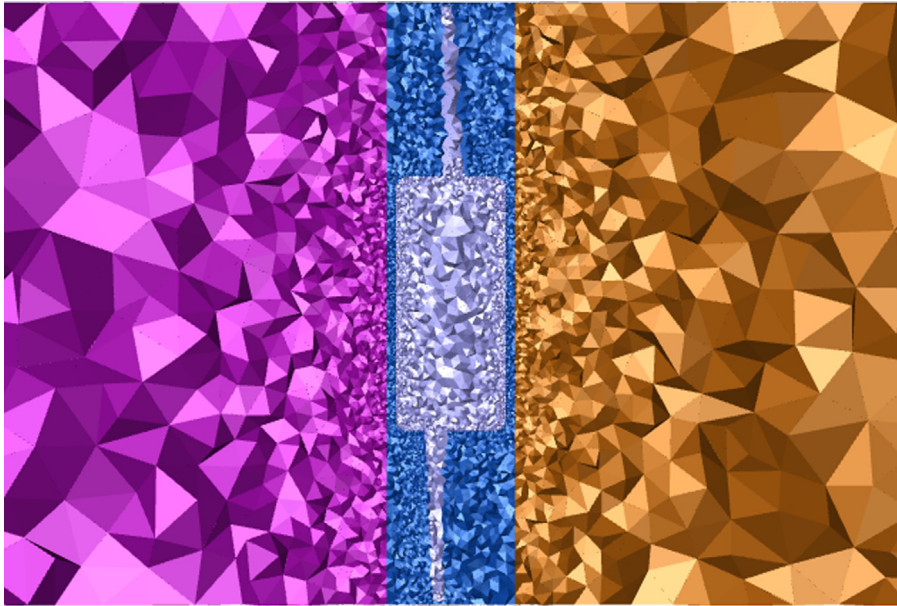


Fig. 5. Localized computational grid.

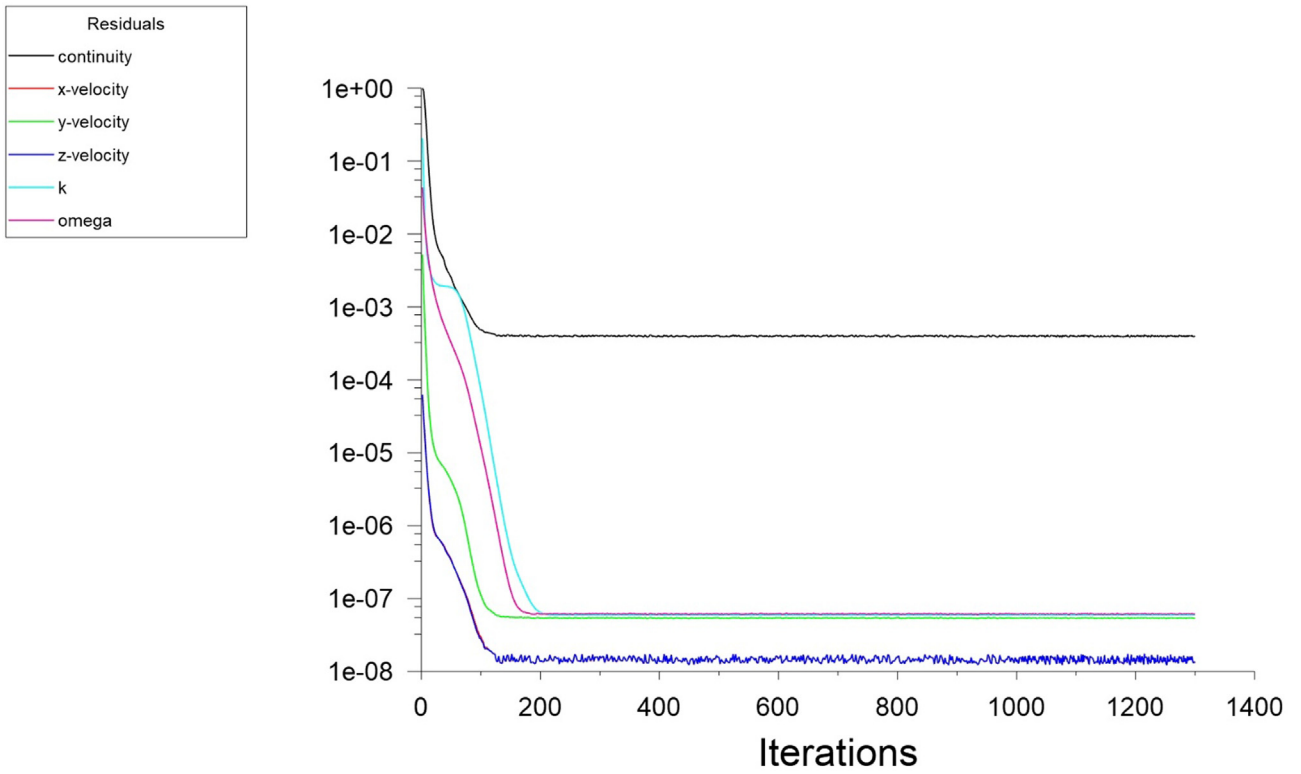
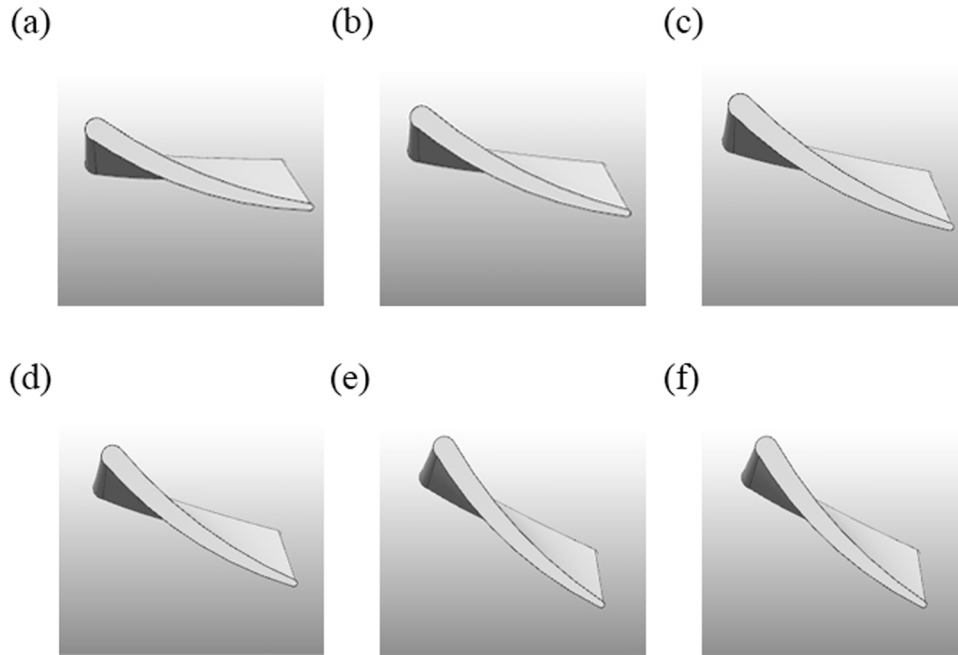


Fig. 6. Convergence curve.

**Table 2.** Optimization results of axial fan.

	Original design	Optimized design	Improvable design
Impeller speed (rpm)	980	1450	*
Blade number	9	8	*
Outlet speed (m/s)	10–15	20–30	Reduced leaf top clearance
Static pressure (Pa)	800–1100	1500–2300	Increase blade curvature
Shaft power (kw)	78	90	*
Noise (dB)	75	69	*
Air volume (m <sup>3</sup> /s)	20.4–32.6	28.6–54.8	Increase blade deflection



**Fig. 7.** Blade mounting angle. In Figure 7, (a) is a partial view of the fan with a mounting angle of 0°; (b) is a partial view of the fan with a mounting angle of 5°; (c) is a partial view of the fan with a mounting angle of 10°; (d) is a partial view of the fan with a mounting angle of 15°; (e) is a partial view of the fan with a mounting angle of 20°; and (f) is a partial view of the fan with a mounting angle of 25°.

respectively;  $\nabla$  is an expression for the dispersion. Therefore, for fluids that are incompressible in nature, their volume tends to remain constant, and is therefore suitable for constant as well as inconstant fluids.

#### 4.2 Law of conservation of momentum

The momentum equation is also known as the N-S (Navier-Stokes) equation, and the law of conservation of momentum is suitable for all fluid problems. The momentum conservation equations in the X, Y, and Z directions in fluid dynamics are shown in equations (5a), (5b), (5c).

$$\frac{\partial(\rho u)}{\partial t} + \text{div}(\rho u V) = \rho f_x + \frac{\partial \tau_{xx}}{\partial x} + \frac{\partial \tau_{xy}}{\partial y} + \frac{\partial \tau_{xz}}{\partial z} - \frac{\partial P}{\partial X}, \quad (5a)$$

$$\frac{\partial(\rho v)}{\partial t} + \text{div}(\rho v V) = \rho f_y + \frac{\partial \tau_{xy}}{\partial x} + \frac{\partial \tau_{yy}}{\partial y} + \frac{\partial \tau_{yz}}{\partial z} - \frac{\partial P}{\partial y}, \quad (5b)$$

$$\frac{\partial(\rho w)}{\partial t} + \text{div}(\rho w V) = \rho f_z + \frac{\partial \tau_{xz}}{\partial x} + \frac{\partial \tau_{yz}}{\partial y} + \frac{\partial \tau_{zz}}{\partial z} - \frac{\partial P}{\partial z}. \quad (5c)$$

In equations (5a), (5b), (5c),  $V$ —denotes the velocity vector;  $\rho$ —for density;  $f_x, f_y, f_z$ —denotes the component of the volume force on the micrometric body in the X, Y, Z axes;  $\tau_{xx}, \tau_{xy}, \tau_{xz}$ —Component of viscous stress  $\tau$  on the surface of the micrometabolite in each coordinate axis;  $P$ —represents the pressure on the micrometric body. When the volumetric force is acting only by gravity, at that point the  $f_x = f_y = 0, f_z = g$ .

### 4.3 Law of conservation of energy

The energy conservation equation is shown in equation (6).

$$\frac{\partial}{\partial t} \left[ \rho \left( e + \frac{v^2}{2} \right) \right] + \nabla \cdot \left[ \rho \left( e + \frac{v^2}{2} \right) \right] = 0$$

$$\frac{\partial}{\partial x} \left( \frac{k}{c_p} \frac{\partial T}{\partial x} \right) + \frac{\partial}{\partial y} \left( \frac{k}{c_p} \frac{\partial T}{\partial y} \right) + \frac{\partial}{\partial z} \left( \frac{k}{c_p} \frac{\partial T}{\partial z} \right) + S_T = 0. \quad (6)$$

In equation (6),  $e$ —represents the internal energy per unit mass due to molecular motion;  $S_T$ —represents the heat from the viscous force.

## 5 Simulation results

Through the Finite Volume Simulation approach described in the previous section, the processed model was batch imported into Fluent for computation and the data was processed in the post-processing module CFD-Post. The cloud diagrams of the axial fan blade pressure, the state of the flow field inside the axial fan, and the import and export velocities in the computational domain of the axial fan were obtained through the setup, and the parameters such as the shaft power were obtained through the computation. A comparison of the original design with the optimized design results is shown in Table 2. In view of the use environment of the axial fan used in this study, it is necessary to consider the result error brought by the underground scene, but the error is found to be within the controllable range through data comparison, so the results of this study are valid.

### 5.1 Simulation of mounting angles

Blades mounting angle plays a crucial factor for fan power as well as efficiency, and simulation optimization of the mounting angle is needed to determine the optimal mounting angle size interval when designing the fan, so as to design the fan with more performance by combining the conditions of other variables. Therefore, six sets of mounting angle parameters were designed in this study to verify the importance of the mounting angle as shown in Figure 7, and the optimized optimal size of the mounting angle was obtained as a fixed parameter in the subsequent simulation.

### 5.2 Mounting angle simulation results

As can be seen in Figure 8, the P-Q performance curve of the fan shows a linear increase or decrease with the increase of the mounting angle, starting from 0° to 20°, the outlet static pressure of the fan increases significantly, and after reaching 20° the static pressure begins to decrease, but are greater than 1° to 15°, in addition to the flow rate of the fan and the static pressure shows the same trend. Figure 8b clearly shows that the installation angle at 20° both parameters reached the maximum value. Therefore, from the simulation results, it can be seen that the blade mounting angle at 20° is suitable for the fan used in this study.

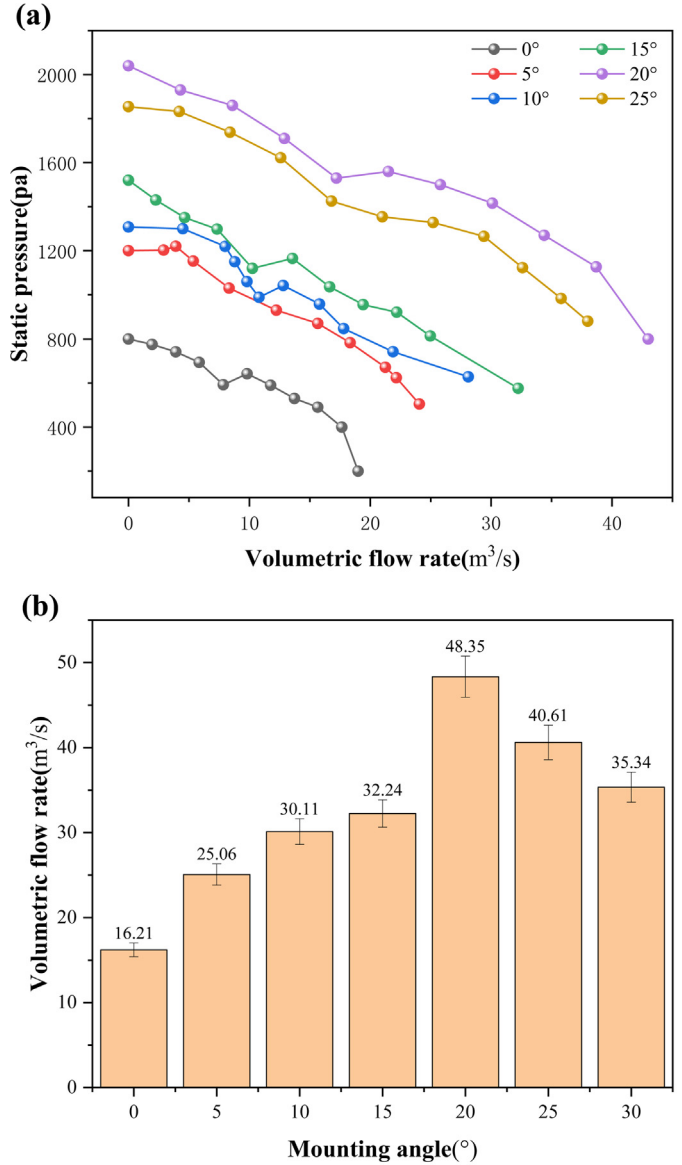
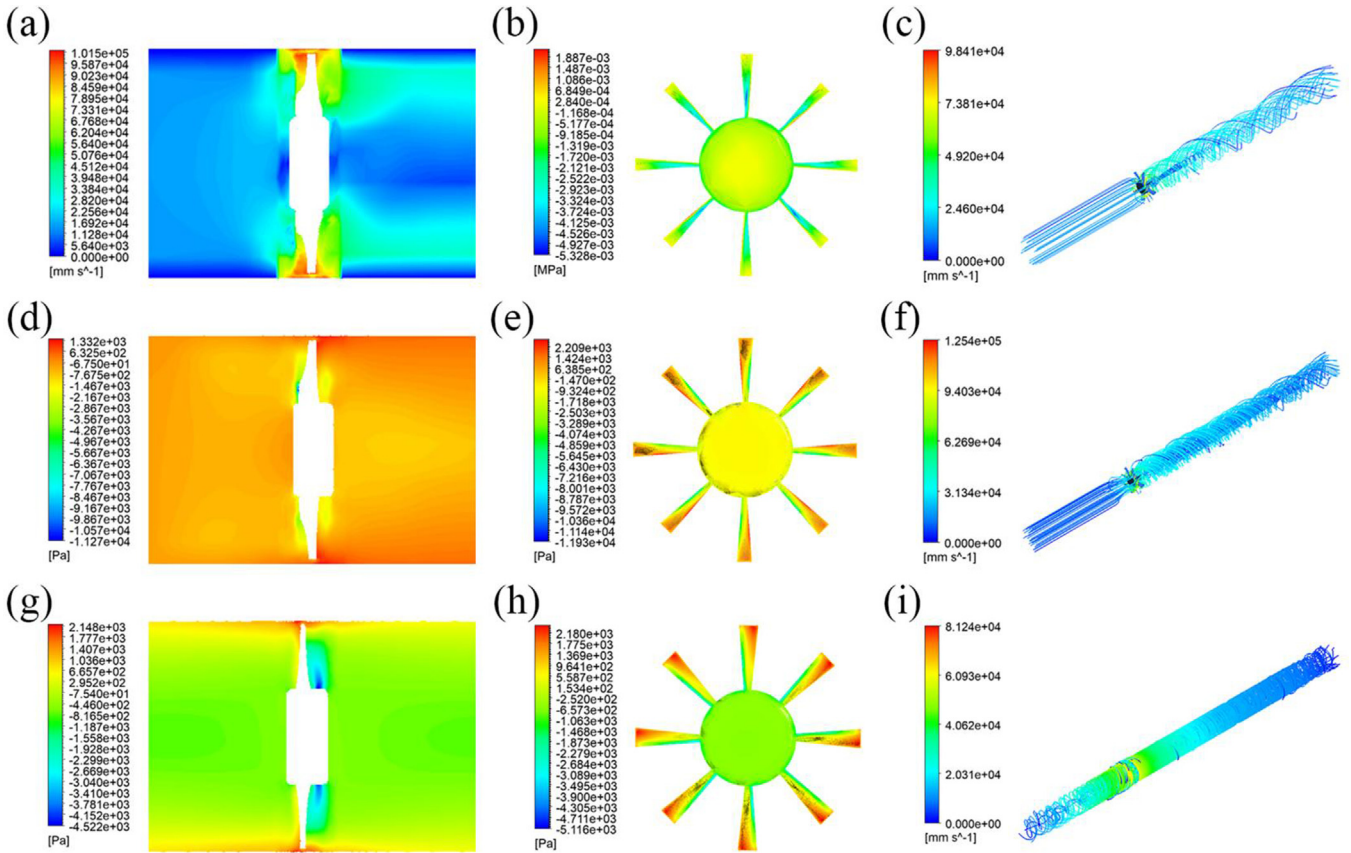


Fig. 8. Mounting angle simulation results.

As can be seen from Figure 9, the installation angle of the fan blade in the characteristic values of 15°, 20°, 25°, the pressure on the impeller at (a) (d) (g) shows a trend of increasing and then decreasing, but for the (a) (g) two kinds of installation angle have appeared in the tip of the blade of the impeller blade pressure is much larger than the other parts of the phenomenon. In the (b)(e)(h) impeller pressure maps, the pressure on the blades and impeller in (b) is numerically smaller than that in (e)(h), but there is a pressure surge area and the static pressure and flow rate provided are smaller than the latter two. (c) (f) (i) velocity line graph, the installation angle of 20° when the air flow rate between the blades is significantly greater than its and both, then the exit velocity and flow rate provided are greater than its and both. To summarize the above, 20° mounting angle can be taken as the structural parameter of the axial flow fan for mining in this study.





**Fig. 9.** Static pressure velocity cloud for blade mounting angle. In Figure 9, (a)–(c) shows the hydrostatic velocity cloud at a mounting angle of 15°; (d)–(f) shows the hydrostatic velocity cloud at a mounting angle of 20°; and (g)–(i) shows the hydrostatic velocity cloud at a mounting angle of 25°.

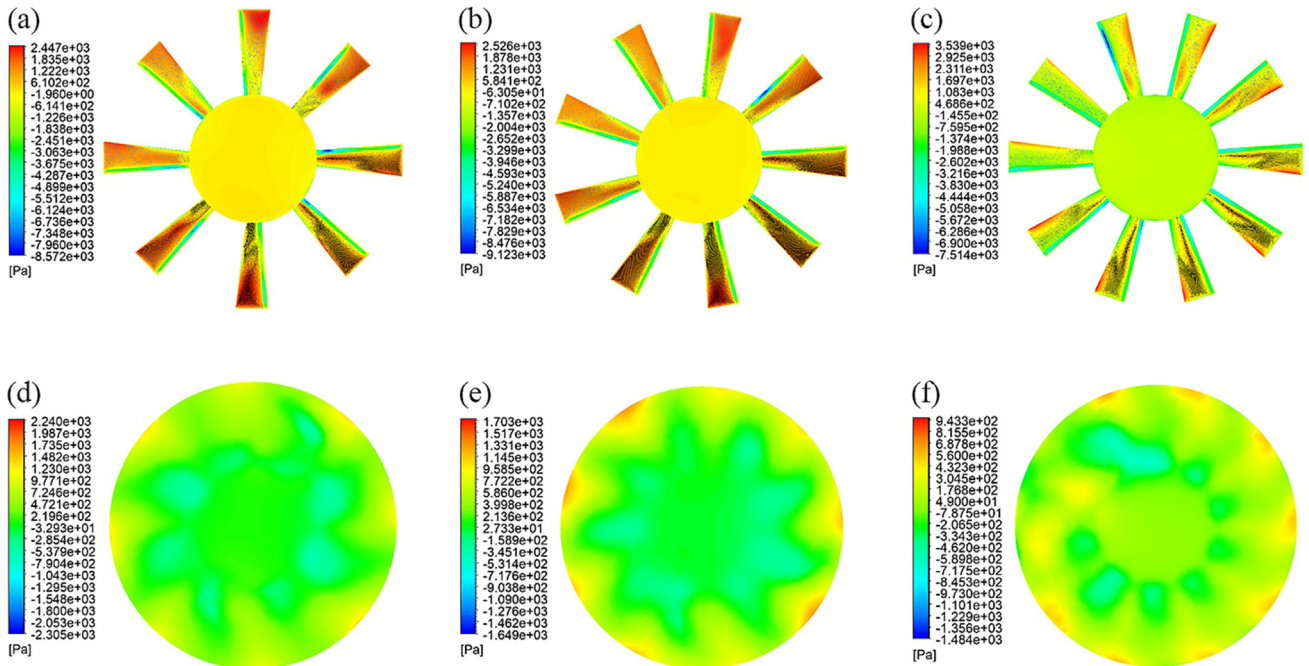


**Fig. 10.** Cloud view of blade number simulation results. In Figure 10, (a) shows the 8-blade results and scale; (b) shows the 9-blade results and scale; (c) shows the 10-blade results and scale; (d) shows the pressure distribution in the rotational domain of the 8-blade; (e) shows the pressure distribution in the rotational domain of the 9-blade; and (f) shows the pressure distribution in the rotational domain of the 10-blade.

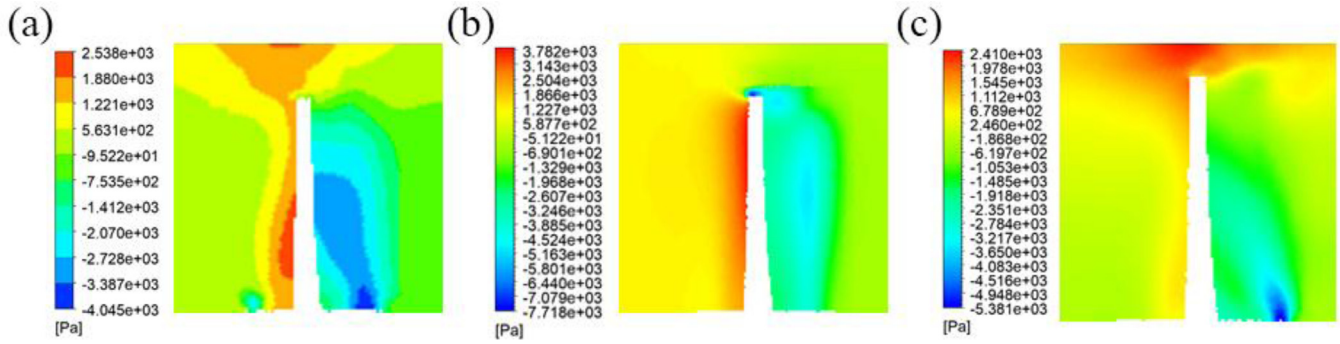


**Fig. 11.** Pressure cloud of blade number blades. In Figure 11, (a)–(c) shows the pressure cloud diagram of the blades of 10, 9, 8 blade wind turbine respectively.

From the results of the mounting angle simulations, it can be seen that the performance of the fan with a mounting angle of 20° reaches its maximum value and runs smoothly in this section of the study, but there are also corresponding disadvantages. Although the maximum flow rate and static pressure of the fan designed in this study are achieved at a mounting angle of 20°, the safe operating zone of the fan is very small, and this design needs to be further optimized for commercial fans, so the following section will continue to optimize the performance of commercial fans in the structure.

### 5.3 Simulation of the number of blades

When the axial fan operates, the work done by the blades on the airflow makes the gas flow from the inlet end to the outlet end, thus exchanging the old and new air and providing fresh air for the underground mine. Its air volume and pressure are closely related to the number of blades. Therefore, the number of blades becomes a crucial factor affecting its performance. In this study, three kinds of axial fans with 8, 9 and 10 numbers of blades were designed and analyzed, and the pressure on the blades and the pressure distribution in the fluid domain brought about by the change of the number of blades were obtained. The optimum number of blades is selected for the next study.

### 5.4 Results of blade number simulation

In the study of blades, from Figures 10a–c it can be seen that the 8-blade fan blade is subjected to the smallest positive pressure, in the fluid domain of the fan 9 blade and 10 blade fan fluid domain appeared in the positive pressure surge area and negative pressure to become larger area. In addition, in Figure 11 the 9-blade and 10-blade two structures of the axial fan are blade frontal force, easy to cause the blade tensile surface of the crack fracture, while the 8-blade fan blade belongs to the tip of the force, the pressure suffered by the leaf root is significantly reduced, so the performance is better. The probability of blade failure is small compared to its with two cases. At the same time, there are some prominent variation areas within the fluid domain that are not favorable to the smooth operation of the fan, and combined with the pressure comparison of the

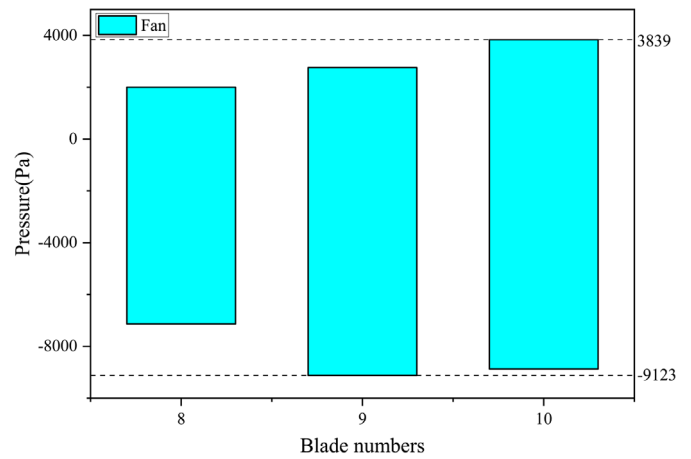


**Fig. 12.** Histogram of blade positive back pressure distribution.

blades in Figure 12, the axial fan with 8 blades installed has a more superior performance in use in the interval, since the unfavorable factors to which it is subjected are significantly less than those of the remaining two configurations. To summarize, in this study, the 8-blade fan is chosen as the final solution and will be the subject of subsequent studies.

### 5.5 Simulation of the deflector shroud

Under the precondition that the mounting angle is 20°, a one-factor simulation method is used to simulate the study of whether the fan is installed with front and rear deflectors, and to derive the changes in the performance of the fan in the case of structural changes, especially when the deflector is installed. After a rigorous simulation program to simulate the axial fan model, it was found that the internal flow field of the fan was most stable when the front deflector was installed, and the control of fan stall was most effective. Secondly, in terms of aerodynamic performance, the fan with front deflector has better aerodynamic performance than the fan without deflector and with both front and rear deflectors and only rear deflector, and the installation of the front deflector is greatly optimized in terms of economy and the weight of the equipment itself.

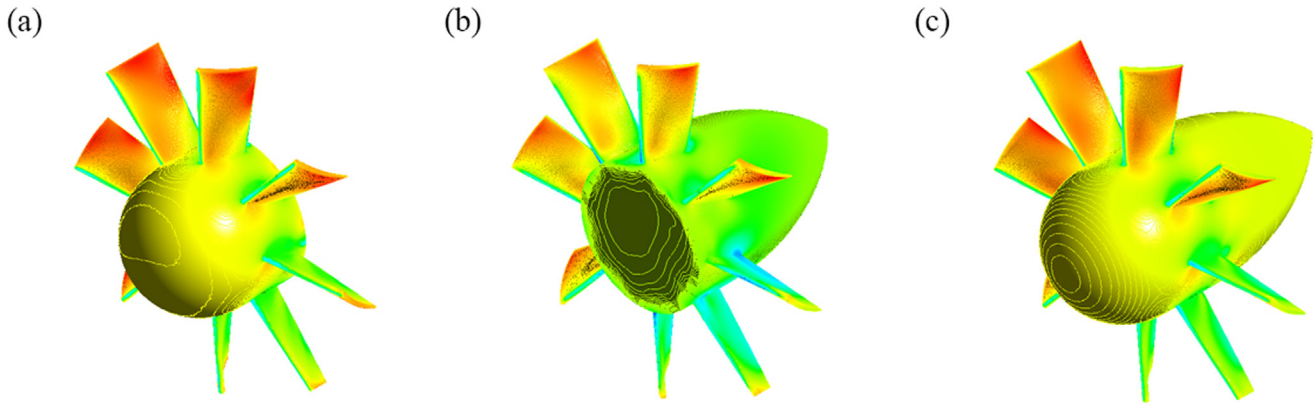


Fig. 13. Cloud view of deflector pressure distribution.

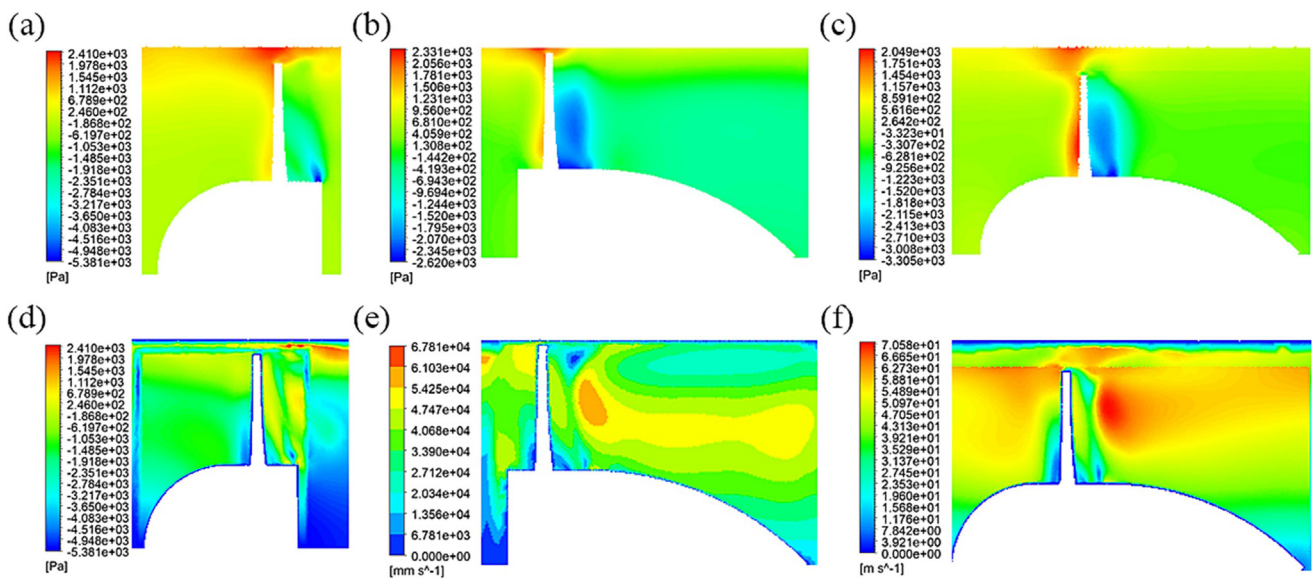


Fig. 14. Pressure and velocity cloud of the fan side view cross-section. In Figure 14, (a) represents the pressure cloud of the rotational domain cross-section of the deflector fan before installation; (b) represents the pressure cloud of the rotational domain cross-section of the deflector fan after installation; (c) represents the pressure cloud of the rotational domain cross-section of the deflector fan before and after installation; (d) represents the velocity cloud of the rotational domain cross-section of the deflector fan before installation; (e) represents the velocity cloud of the rotational domain cross-section of the deflector fan after installation; and (f) represents the velocity cloud of the rotational domain cross-section of the deflector fan before and after installation. (f) represents the cross-section velocity map of the rotating domain of the deflector fan before and after installation.

## 5.6 Numerical simulation results of the deflector shield

The deflector can significantly optimize the fluid flow direction in the fluid domain and improve the aerodynamic performance. In Figures 13a–c, it can be seen that in (a) and (b), the pressure disorder phenomenon occurs in the inlet direction, whereas (c), due to the simultaneous addition of the front and rear deflectors, the pressure is uniformly distributed in the inlet direction, which greatly reduces the damaging effect due to the pressure surge in part of the region. In the blade pressure, (a) in the pressure side of the pressure is much larger than the back pressure side, and in the tip of the pressure surge area; (b) in the back pressure side of the pressure is much larger than

the pressure side, and the pressure is not uniformly distributed in the blade, there are two pressure surge area; only (c) in the distribution of pressure is uniform and numerically less than the first two, so in the rotating area of the fan, the deflector should be selected to install the front and rear deflectors at the same time.

The deflectors in this study are defined as front deflector, rear deflector, and front and rear deflectors. The static pressures exerted on the side section, blade root, middle, and top are monitored respectively, as shown in Figure 14, and analyzed in conjunction with the scale values in (a)–(c), the maximum pressure exerted on the fan with front and rear deflector hoods is less than that of the fan with only front or rear deflector hoods, and the fan with front and rear deflector hoods has a greater velocity in the



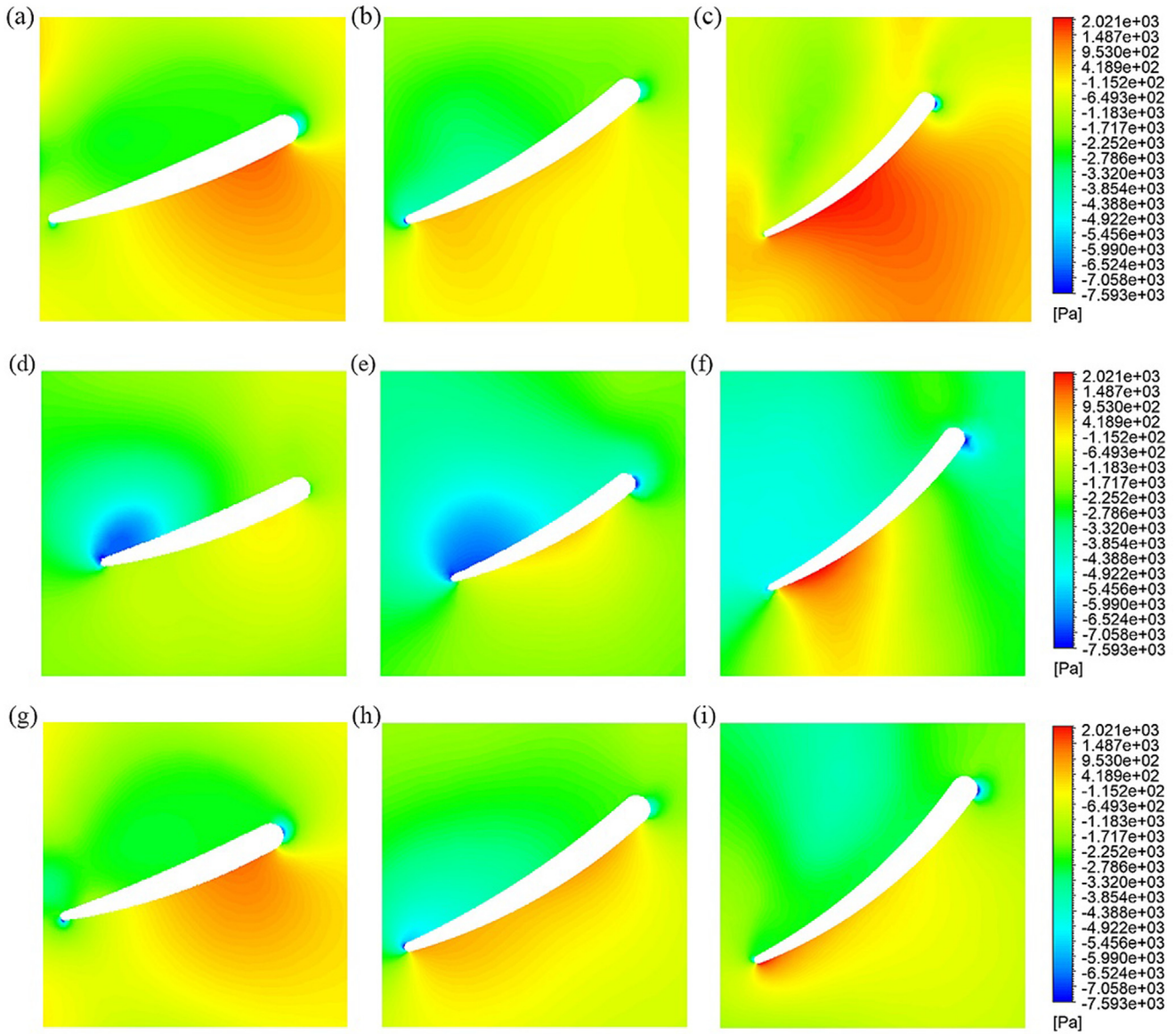


**Fig. 15.** Blade root, center, top pressure distribution. In Figure 15, (a), (d), (g) represent the pressure distribution at the root of the blades of three different deflector fan installations; (b), (e), (h) represent the pressure distribution in the middle of the blades of three different deflector fan installations; and (c), (f), (i) represent the pressure distribution at the top of the blades of three different deflector fan installations, respectively.

velocity cloud diagrams, which implies that he can provide a greater outlet velocity as well as air volume, while the outlet static pressure is also increased. In addition, as shown in Figures 15a–c shows the pressure distribution of the blade of the deflector before installation, Figures 15d–f shows the pressure distribution of the blade of the deflector after installation, and Figures 15g–i shows the pressure distribution of the blade of the deflector before and after installation. It is obvious that the fan blade with the front deflector is subjected to greater back pressure, and the outer side of the blade is adversely affected or even fractured due to the tensile stress on the blade. After the installation of the deflector fan blade root and center to withstand a greater positive pressure, the top of the blade to withstand a greater back pressure, so that the entire blade to withstand a greater torque.

The fan blades with front and rear deflectors are subjected to less positive back pressure than the first two types of fans, and in this study, the main focus is on the blade performance study, therefore, the fan with front and rear deflectors is used as the program of this study for the next step of the study.

### 5.7 Simulation of rotational speed

Combining the results of various parameters required for the mine fan, this study has tried three different rotational speeds to simulate the aerodynamic performance of the fan in conjunction with the results described in the previous section. The fan model used for numerical simulation is a fan with hub diameter of 1320 mm, number of blades 8, and blade mounting angle of 20°, and the simulation results are shown in Figures 16 and 17. Figure 16 combined with Figure 17 in



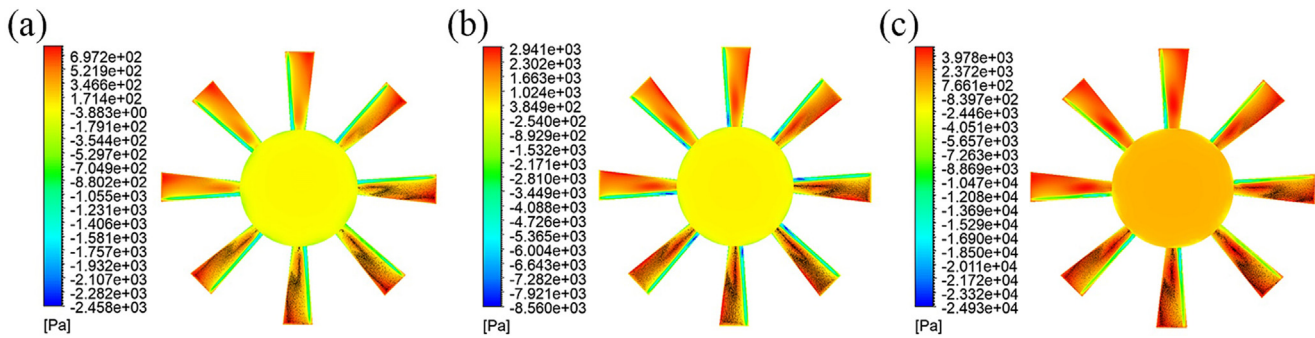


**Fig. 16.** Rotational speed blade pressure cloud. In Figure 16, (a)–(c) represent the simulation results at 1250 rpm, 1450 rpm and 1650 rpm, respectively.

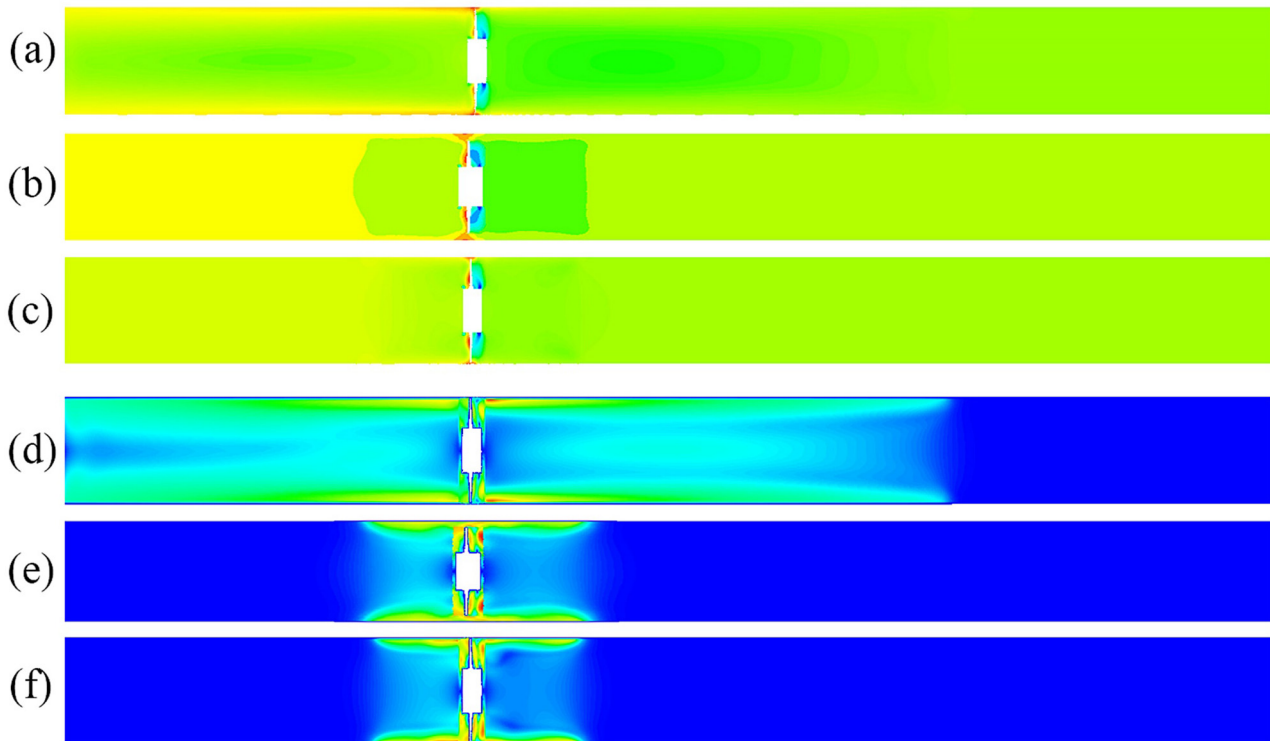


**Fig. 17.** Comparison of rotational speed and pressure. In Figure 17, (a)–(c) represent pressure clouds at speeds of 1250 rpm, 1450 rpm, and 1650 rpm, respectively, and (d)–(f) represent velocity clouds at speeds of 1250 rpm, 1450 rpm, and 1650 rpm, respectively.

(a)–(c) analysis, the blade pressure force is minimum and the outlet speed is maximum. Therefore, a speed of 1450 rpm is selected as the final speed of the fan to be put into development.

## 6 Conclusions

The performance optimization results were obtained by designing and adjusting the parameters of the axial flow fan, and solving various models using finite volume simulation. The advantages of the axial flow fan after numerical simulation optimization are as follows:

Firstly, at a specific installation angle, the axial flow fan exhibits superior performance, with an increase of 4.98% in axial power compared to the maximum outlet static pressure and outlet velocity. The internal airflow component of the axial flow fan has decreased significantly due to the change in installation angle, which increases the velocity of the airflow when escaping the blades and makes the airflow flow more evenly on the blade surface. This is an economical and practical approach, but the structure in this study is not adjustable for moving blades.

Secondly, the number of blades described in this study is a significant innovation, which not only stabilizes the internal flow field of the axial flow fan but also increases the

static pressure of the fan, increasing the safe working area of the axial flow fan. In this study, even numbered blades showed superior performance compared to odd numbered blades.

Again, the axial flow fan can provide sufficient flow and air pressure at lower speeds, but it can produce greater energy when operating at 1450rpm.

Finally, the changed parameters result in less turbulence and noise during operation of the axial flow fan, so the optimized axial flow fan is applicable.

### Acknowledgments

This study was supported by Natural Science Foundation of Shandong Province (ZR2021ME182), State Key Laboratory of Material Forming and Mould Technology Open Fund Project(P12), National Natural Science Foundation of China (52001187), the Science and Technology Enterprise Innovation Program of Shandong Province, China (2023TSGC085, 2023TSGC0119, 2023TSGC0759 and 2023TSGC0961) and Shandong Province Development and Reform Commission Special Needs Talents Project: R&D and Application of Intelligent Manufacturing Key Technology for High Performance Railway Wheel Unit Production Line.

### Funding

The research is supported by JNGC2023001.

### Conflict of Interest

The authors declare that they have no known competing financial interests or personal relationships that could have appeared to influence the work reported in this paper.

### Data availability statement

Data will be made available on request.

### Author contribution statement

Renhui Liu wrote the manuscript and responsible for the experimental work. Shubo Xu wrote the manuscript and responsible for the experimental work. Guocheng Ren and Jianing Li contributed to data extraction and format correction of the article. Kangwei Sun, Xiaoyu Ju and Xiquan Ma contributed to formal analysis. Yuefei Pan, Weihai Zhang and Wenming Wang was responsible for supervision. All the authors read and approved the final manuscript.

### References

1. S.M. Fakhari, H. Mrad, Optimization of an axial-flow mine ventilation fan based on effects of design parameters, *Res. Eng.* **21**, 101662 (2024)
2. C. Tian, X. Liu, J. Wang, G. Xi, Effects of bionic blades inspired by the butterfly wing on the aerodynamic performance and noise of the axial flow fan used in air conditioner, *Int. J. Refrigerat.* **140**, 17–28 (2022)
3. C. Li, Q. Lin, X. Ding, X. Ye, Performance, aeroacoustics and feature extraction of an axial flow fan with abnormal blade angle, *Energy* **103**, 322–339 (2016)
4. V. Sushma Chinta, P. Ravinder Reddy, K. Eshwar Prasad, Investigation of shear properties of axial flow fan blade material with partial woven jute reinforcements, *Mater. Today: Proc* (2023). <https://doi.org/10.1016/j.matpr.2023.02.426>
5. M. Moosania, C. Zhou, S. Hu, Aerodynamics of a partial shrouded low-speed axial flow fan, *Int. J. Refrigerat.* **130**, 208–216 (2021)
6. D. Zhang, R. Chen, Z. Zhang, S. He, M. Gao, Crosswind influence on heat and mass transfer performance for wet cooling tower equipped with an axial fan, *Case Stud. Thermal Eng.* **27**, 101259 (2021)
7. Z. Dang, Z. Zhang, M. Gao, S. He, Numerical simulation of thermal performance for super large-scale wet cooling tower equipped with an axial fan, *Int. J. Heat Mass Transfer* **135**, 220–234 (2019)
8. K.Y. Xiao, F. Pirajno, Y. Xu, S. Zhang, L. Sun, Y. Cong et al., Study on the major minerals potential in China, *Ore Geol. Rev.* **127**, 103816 (2020)
9. X.Z. Xu, K.Q. Wang, Q.H. Zhang, Y.H. Yao, A comprehensive evaluation of intelligent coal mine ventilation systems in the internet of things, *Human-Centric Comput. Inform. Sci.* **13**, 46 (2023)
10. T.C. Yang, X.L. Chen, H.M. Cheng, Aerodynamic performance analysis of axial-fan in low pressure pipeline based on ANSYS CFX, in *Proceedings of the 2015 Joint International Mechanical, Electronic and Information Technology Conference (JIMET 2015)* (2015)
11. T. Hemant Kumawat, Modeling and Simulation of Axial Fan Using CFD (2015)
12. J. Wang, N.P. Kruyt, Computational fluid dynamics simulations of aerodynamic performance of low-pressure axial fans with small hub-to-tip diameter ratio, *J. Fluids Eng.* **142** (2020). doi: [10.1115/1.4047120](https://doi.org/10.1115/1.4047120)
13. Y. Liu, Z. Lin, P.F. Lin, Y.Z. Jin, T. Setoguchi, H.D. Kim, Effect of inlet guide vanes on the performance of small axial flow fan, *J. Thermal Sci.* **26**, 504–513 (2017)
14. K.M. Munisamy, R. Govindasamy, S.K. Thangaraju, Experimental and numerical investigation onto 1250mm axial fan, in *Aerotech IV: Recent Advances In Aerospace Technologies* (2012)
15. Y.J. Wu, D.G. Huang, Optimization design of axial fan blade, *J. Chin. Inst. Eng.* **42**, 473–478 (2019)
16. S.H. Liu, R.F. Huang, L.J. Chen, Performance and inter-blade flow of axial flow fans with different blade angles of attack, *J. Chin. Inst. Eng.* **34**, 141–153 (2011)
17. Z.B. Yu, Z.C. Liu, X.Y. Gao, S.X. You, Structure design of a new-style moving blade adjusted axial fan, in *Proceedings of the 5th International Conference on Advanced Design and Manufacturing Engineering* (2015)
18. L. Diao, F. Ge, Y. Liu, L. Yang, Y. Liu, Q. Huang, Effect of tip winglet position on tip flow and noise of axial flow fan, *Heliyon* **9**, e18483 (2023)
19. G.L. Podgajetsky, M.L.C. de Oliveira, C.J.L. Hermes, Model-based efficiency mapping and parametric analysis of low-pressure axial fans, *Int. J. Refrigerat.* **144**, 136–144 (2022)
20. R. Salcedo, A. Fonte, M. Grella, C. Garcera, P. Chueca, Blade pitch and air-outlet width effects on the airflow generated by an airblast sprayer with wireless remote-controlled axial fan, *Comput. Electr. Agric.* **190**, 106428 (2021)
21. A. Pogorelov, M. Meinke, W. Schröder, Effects of tip-gap width on the flow field in an axial fan, *Int. J. Heat Fluid Flow* **61**, 466–481 (2016)
22. X. Ye, P. Li, C. Li, X. Ding, Numerical investigation of blade tip grooving effect on performance and dynamics of an axial flow fan, *Energy* **82**, 556–569 (2015)
23. S.M.A. Moghadam, M. Meinke, W. Schröder, Analysis of tip-leakage flow in an axial fan at varying tip-gap sizes and operating conditions, *Comput. Fluids* **183**, 107–129 (2019)
24. Y.-M. Li, Z.-N. Zhou, Investigation and numerical simulation of inner-flow of an axial mineflow fan under low flow rate conditions, *J. China Univ. Mining Technol.* **18**, 107–111 (2008)

25. Y. Ding, J. Wang, B. Jiang, Q. Xiao, X. Yang, L. Wu, B. Xie, Numerical investigation of the effect of blade distortion laws on the corner flow separation of the axial-flow fan, *Aerospace Sci. Technol.* **138**, 108296 (2023)
26. B. Luo, W. Chu, H. Zhang, Tip leakage flow and aeroacoustics analysis of a low-speed axial fan, *Aerospace Sci. Technol.* **98**, 105700 (2020)
27. A. Shahsavari, M. Nili-Ahmadabadi, A novel approach for the design of axial flow fan by increasing by-pass ratio in a constant-diameter turbofan, *Propuls. Power Res.* **9**, 142–158 (2020)
28. X. Liu, J. Liu, D. Wang, L. Zhao, Experimental and numerical simulation investigations of an axial flow fan performance in high-altitude environments, *Energy* **234**, 121281 (2021)
29. W. Yang, Y. Wu, S. Liu, An optimization method on runner blades in bulb turbine based on CFD analysis, *Sci. China Technol. Sci.* **54**, 338–344 (2011)
30. P. Ma, J. Wang, H. Wang, Investigation of performances and flow characteristics of two bi-directional pumps with different airfoil blades, *Sci. China Technol. Sci.* **61**, 1588–1599 (2018)

**Cite this article as:** Renhui Liu, Shubo Xu, Kangwei Sun, Xiaoyu Ju, Weihai Zhang, Wenming Wang, Xiquan Ma, Yuefei Pan, Jianing Li, Guocheng Ren, CFD analysis and optimization of axial flow fans, *Int. J. Simul. Multidisci. Des. Optim.* **15**, 11 (2024)